NENE
International Conference
Nuclear Energy for New Europe

Advanced Analytical and Numerical Modelling of ATF *FeCrAl* and *Cr*-Coated *Zr*-Based Cladding High Temperature Oxidation in Steam Atmosphere

Alexander Vasiliev
Nuclear Safety Institute (IBRAE)
B.Tulskaya 52
115191 Moscow, Russia
vasil@ibrae.ac.ru

ABSTRACT

Currently, the use of perspective advanced tolerant fuel (ATF) claddings is considered as one of encouraging ways to strengthen the reliability, safety and performance of nuclear fission generation.

Several perspective ATF cladding candidates are chosen for possible application in commercial nuclear power plants (NPPs) in the world including a cladding from *FeCrAl* alloy and zirconium-based cladding with protective chromium coating (*Zr*/*Cr* cladding).

The *FeCrAl* alloy and chromium have excellent characteristics of corrosion and oxidation resistance compared to zirconium both for the NPP normal operation temperatures and high-temperature conditions. It is very important for the nuclear safety including the resistance to design-basis and beyond-design-basis accidents at NPPs.

However, the worsening of *FeCrAl* cladding oxidation characteristics is reported when approaching the melting temperature of *FeO* (T=1371°C). The formation of melt leads to acceleration of oxidation and hydrogen generation. Also, recent experimental data showed that in the temperature range close to upper limit of design-basis accident (T=1200°C) and higher there is a considerable worsening of *Zr*/*Cr* cladding protective properties. In particular, a role of *Cr-Zr* interdiffusion with subsequent influence on degradation of protective properties is revealed.

In this paper, the new advanced models of high-temperature oxidation of FeCrAl and Zr/Cr cladding are developed. In particular, the Zr/Cr cladding oxidation model is based on simultaneous solution of oxygen and zirconium diffusion equations in different layers of the cladding. A very important role of Zr outward diffusion to the interface between chromium oxide and metallic chromium resulting to severe degradation of protective properties is discovered recently. This phenomenon is taken into account in the model. The models are implemented to newly developed severe accident computer running code.

The comparison of calculated results for FeCrAl and Zr/Cr cladding high temperature oxidation with available experimental data is conducted. The reasonable agreement between calculated and experimental data is observed.

Despite the existence of obvious mechanisms leading to loosing of protective properties at high temperatures, one can make a conclusion that the application of FeCrAl and chromium-coated Zr-based cladding may be optimistic for considerable upgrade of safety level for NPPs especially for design-basis-accident conditions.

1 INTRODUCTION

Nowadays, the keen competition between nuclear energy and other friendly, sustainable and renewable energy resources like solar, wind, geothermal energy etc. is unfolding in search for clean carbon-free world. This competitive development is expected to continue in future decades with safety concern as a major priority. In a postulated loss-of-coolant accident scenario, a nuclear reactor scram reduces fission power generation in the core but heat generation continues by radioisotope decay. Due to the fact that standard Zr-based claddings of fuel elements are characterized by strong exothermic oxidation, the decay heat can lead to rapid temperature increase (escalation) and core degradation.

New perspective types of fuel and fuel element claddings for nuclear reactors can, in particular, eliminate the transition from the design-basis stage of an accident to the beyond-design-basis stage, or increase the transition time from the design-basis stage to the beyond-design-basis and severe accident stage compared to the standard UO_2 fuel/Zr-based alloy cladding system. It seems that the most promising candidates for possible application in ATF-claddings for nuclear reactors in nearest future are as following [1-10]:

- the *Zr*-based alloys with *Cr* coating with thickness about 10÷15 μm;
- the iron-chromium-aluminium alloy *FeCrAl*;
- the non-metallic ceramics *SiC*;
- the *C*r-*Ni* alloys.

The oxidation parabolic kinetics of those materials in comparison to standard basic material used currently in nuclear industry are shown in Fig. 1 [1-10].

In this paper, we consider modelling of high-temperature oxidation behavior of *FeCrAl* and *Zr*/*Cr* claddings. It is seen in Fig. 1 that the *FeCrAl* and a chromium reveal very good corrosion and oxidation kinetics characteristics which are lower by almost two orders of magnitude compared to *Zr*-based alloy claddings. So, it is expected that *the both FeCrAl* and *Zr*/Cr cladding should be good candidates for application in commercial nuclear reactors.

The Zr/Cr cladding oxidation model was developed recently in the paper [11]. However, new experimental data showed some important features which need to be taken into account in a new advanced model.

Those recent experimental data [2,12] discovered that outstanding oxidation resistance properties relevant of Zr/Cr cladding experience a considerable worsening when approaching temperatures about 1200°C, that is, significantly lower than the melting point of chromium. This is due to a number of factors. First, the formation of cracks in the oxide layer takes place. This phenomenon occurs as a result of the development of mechanical stresses in growing oxide. The main reason for it is the large difference of molar volumes of metal *Cr* and oxide Cr_2O_3. Second, it seems out that *Zr* atoms diffuse into the metallic chromium coating layer resulting in progressive growth of the precipitates of ZrO_2. In this turn, it leads to effective oxygen diffusion coefficient enhancement in metal chromium layer. The reason for it is the fact that the oxygen diffusion proceeds faster along the *ZrO*2 grain boundaries. Third, when *Zr* atoms migrate through metallic *Cr* layer to reach Cr_2O_3/Cr interface, the chemical reaction of *Zr* with Cr_2O_3 (the redox reaction) begins resulting to formation of ZrO_2 and *Cr*. So, this reaction leads to thinning of Cr_2O_3 layer and to growth of metallic *Cr* layer. Obviously, the protective properties of Cr_2O_3 will gradually worsen once again.

Concerning *FeCrAl* cladding oxidation, it was observed in the experiments [8] that the oxidation is considerably enhanced when the temperature approaches about 1250°C÷1400°C that is close to the melting temperature of *FeO*. It is expected that due to relatively low melting temperature of protective oxide layer (with *FeO* as a major part) we encounter high oxidation rate in this temperature range as compared to solid oxide protective layer.

In this paper, the basic equations of advanced *FeCrAl* and Zr/Cr claddings oxidation model are considered describing the phenomena mentioned above. The corresponding

numerical module is developed. The comparison of model predictions with the results of recent experimental tests conducted in KIT, Karlsruhe, Germany, is given. Finally, the main conclusions are made on the basis of results obtained.

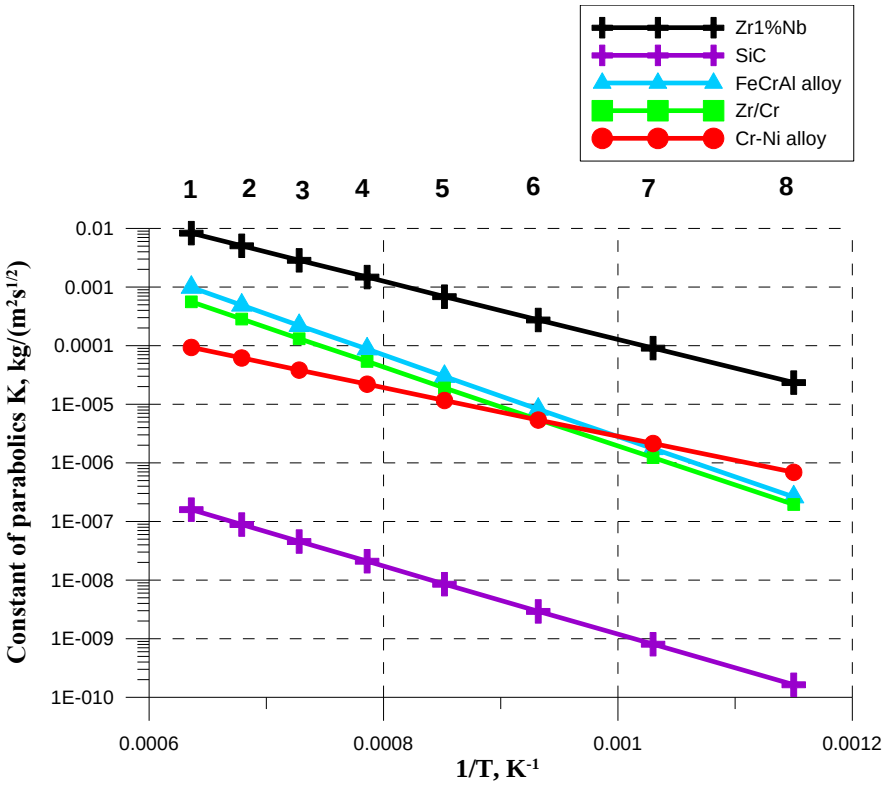

Figure 1: The parabolic oxidation kinetics for different perspective ATF-claddings materials. 1 - 1300°C, 2 - 1200°C, 3 - 1100°C, 4 - 1000°C, 5 - 900°C, 6 - 800°C, 7 - 700°C, 8 - 600°C

2 DESCRIPTION OF CHARACTERISTIC PHASES OF ZR/CR CLADDING HIGH TEMPERATURE OXIDATION AND APPROACHES TO MODELLING

On the basis of experimental results [2,12], three characteristic phases are relevant for the oxidation of claddings made of the *Zr*-based alloys with *Cr* coating:

- metal chromium oxidation in a system Cr_2O_3/Cr (Fig. 2);
- transient phase with progressive growth of oxidation (Fig. 3);
- oxidation in three-layer system ZrO_2/α-*Zr*(*O*)/β-*Zr* after worsening and loss of protective properties in a system Cr_2O_3/Cr (Fig. 4).

We consider now above-mentioned phases.

2.1 Phase I. Oxidation in a system Cr_2O_3/Cr

The initial phase of high-temperature oxidation of *Zr*/Cr cladding corresponds to oxidation of metal chromium (Fig. 1) and it is characterized by parabolic law. We can write the oxygen diffusion equations for a two-layer system Cr_2O_3/*Cr* analogously as in the paper [13] where a two-layer system ZrO_2/α-*Zr*(*O*) was considered.

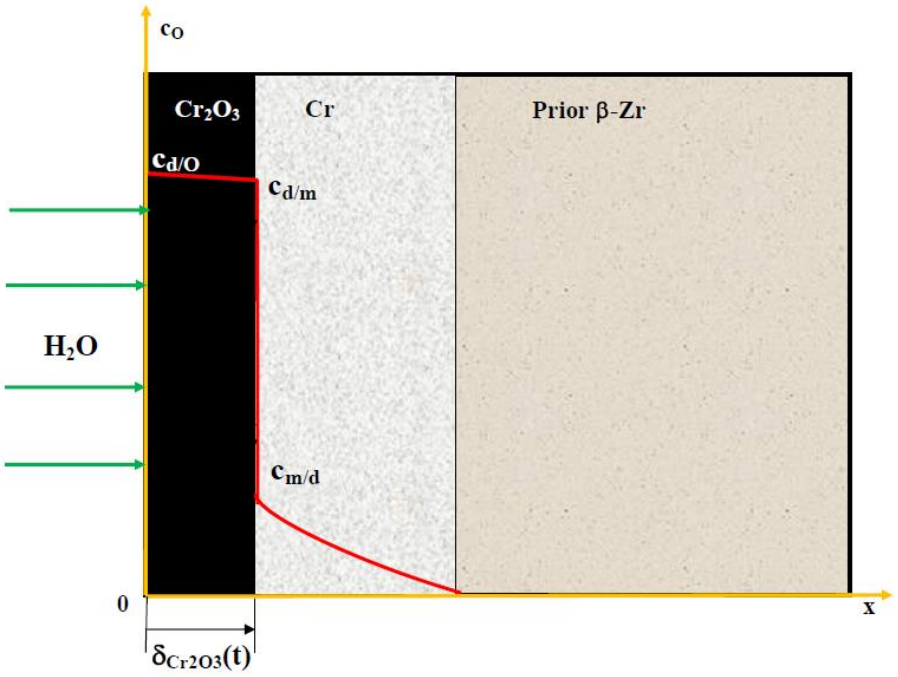

Figure 2: The profile of oxygen concentration in the course of phase I

We can describe the parabolic kinetics for Cr_2O_3 thickness by following equations:

$$\delta_{Cr_2O_3} = \sqrt{k_p t} = K_{ox}\sqrt{t}\,, \tag{1}$$

$$\frac{K_{ox}}{\sqrt{4D_{ox}}} \cong \frac{\left[\sqrt{\frac{4c_{md}\cdot c_{md}}{\pi}+8\frac{D_{ox}}{D_m}\left(c_{\frac{d}{m}}-c_{\frac{m}{d}}\cdot r_{Cr}\right)\cdot\left[c_{\frac{d}{O}}-c_{\frac{d}{m}}\right]}-\frac{2c_{\frac{m}{d}}}{\sqrt{\pi}}\right]}{4\sqrt{\frac{D_{ox}}{D_m}}\cdot\left(c_{\frac{d}{m}}-c_{\frac{m}{d}}\cdot r_{Cr}\right)}\,. \tag{2}$$

Here c_O is the oxygen density in the cladding [kg/m^3], K_{ox} [m/s$^{1/2}$] and $k_p = K_{ox}^2$ [m^2/s] – oxidation parabolic constants, D_{ox} and D_m – the oxygen diffusion coefficients in oxide and metal phases respectively, $c_{d/O}$, $c_{d/m} \cong c_{d/O}$ and $c_{m/d}$ – the interphase concentrations which can be obtained from the binary phase diagram *Cr-O*. The parameter r_{Cr} is equal to $r_{Cr} = \left(\rho_{Cr_2O_3}/\rho_{Cr}\right)\cdot\left(2\mu_{Cr}/\mu_{Cr_2O_3}\right)$ (the Bedworth-Pilling ratio). Note, that the value $c_{m/d}$ is very small compared to $c_{d/m}$. It results from the fact that the solubility of oxygen in solid chromium is very low.

The oxidation constant k_p is approximated by

$$k_p = 4.83\cdot 10^{-5}\cdot e^{-\frac{31228}{T}}\ \text{m}^2/\text{s} \tag{3}$$

according to the experimental data from [2].

We should note that the protective layer Cr_2O_3 is dense at this phase of oxidation. It means that the oxidation kinetics is parabolic. So, very exclusive protective properties of chromium coating are potentially characteristic for Phase I.

2.2 Transition phase

This transient phase is characterized by progressive worsening of chromium coating protective properties. It occurs via enhancement of effective oxygen diffusion rate through Cr_2O_3 layer due to spallation and cracks/pores formation in Cr_2O_3 layer. The appearance of cracks is connected with strong mechanical stress formation in the process of chromium oxide growth. Besides that, the oxygen diffusion in metal Cr layer is also getting more intensive due to enhanced oxygen ions diffusion along growing *ZrO*2 precipitates grains boundaries. In this turn, the formation of *ZrO*2 in Cr_2O_3 is caused by diffusion of zirconium into the chromium layer and further to the boundary between the layers of chromium oxide and metallic chromium which leads to redox reaction $3Zr+2Cr_2O_3=3ZrO2+4Cr$. Also, the intermetallic layer *ZrC*r2 (with thickness of several μm) is formed between *Zr* and *Cr* layers [2].

When atoms of *C*r from Cr_2O_3 are replaced by Zr atoms, the protective chromium oxide layer is diminished (dissolved). Thus, the unexpected thinning of Cr_2O_3 is very important factor leading to drastic worsening of Cr_2O_3 protective properties.

As a result, the oxidation of *Zr* substrate is observed leading to the growth of the α-*Zr*(*O*) layer at this phase due to intensive oxygen diffusion through both Cr_2O_3 and *Cr* layers (Fig. 4).

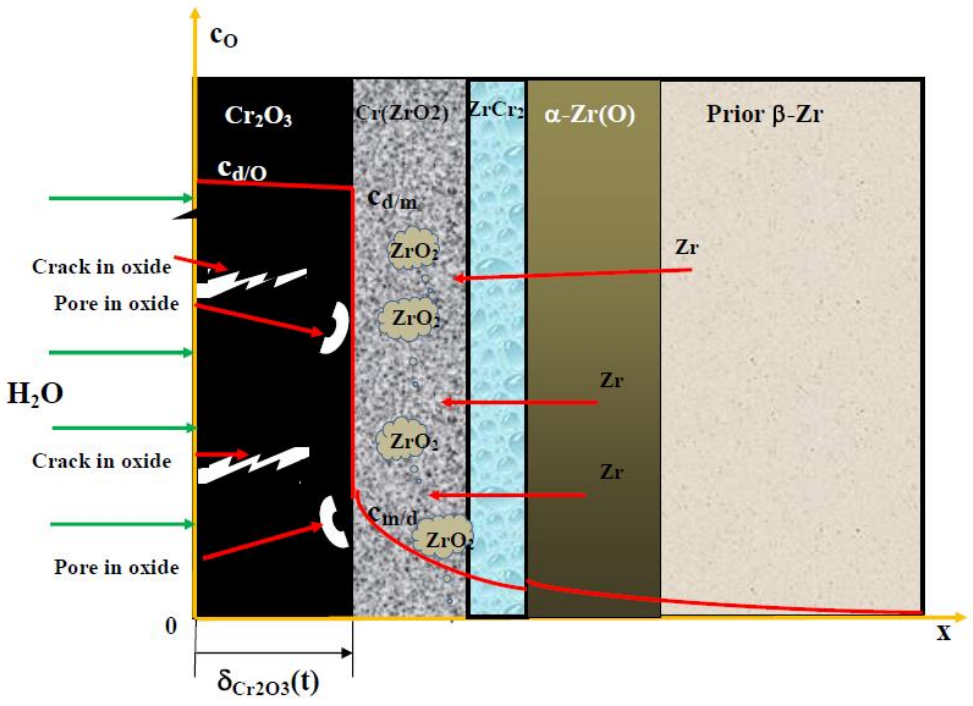

Figure 3: The profile of oxygen concentration in the course of phase II

The main equations describing these phenomena are written as follows. The oxygen diffusion flux through Cr_2O_3 layer is equal to

$$J_O = D_{ox}\frac{(c_{d/O}-c_{d/m})}{\delta_{Cr_2O_3}}\,. \tag{4}$$

Then, the numerical routine to calculate the chromium oxide thickness dynamics $\delta_{Cr_2O_3} = \mathrm{d}$ in time is written below:

$$d^{n+1} = d^n + K_{d1}\tau - J_{cr}^n\frac{n\tau}{\rho_{Cr_2O_3}}\,, \tag{5}$$

where

$$J_{Cr} = \frac{4}{3}J_{Zr}\,, \qquad J_{Zr} = -D_{Zr}A/d_{Cr}\,, \qquad K_{d1} = \frac{J_O\mu_{Cr_2O_3}}{\mu_O\rho_{Cr_2O_3}}\,. \tag{6}$$

The upper subscript n in variable d^n denotes the number of time steps, τ - is the time step. The parameter K_{d1} describes the oxide thickness increment during one time step, J_{Zr} – the zirconium diffusion flux through metallic chromium layer, J_{Cr} – the chromium flux from the Cr_2O_3 layer to the *Cr* layer due to redox reaction, d_{Cr} – the metallic chromium layer thickness, *A* – the empirical constant.

2.3 Loss of chromium protective properties

After partial and then complete exhaustion of protective properties, the oxidation of Zr-based substrate will take place (Fig. 4). It means that the well-known oxidation of zirconium in three-layer configuration (for temperatures *T*>1136K) or in two-layer system (*T*<1136K) will begin [13]. The three-layer system has the following material layers: ZrO_2, α-*Zr*(*O*) and β-*Zr*. In two-layer system only ZrO_2 and α-*Zr*(*O*) are present.

Once again, to calculate the oxidation kinetics we need to solve oxygen diffusion equations in zirconium three- or two-layer system [13].

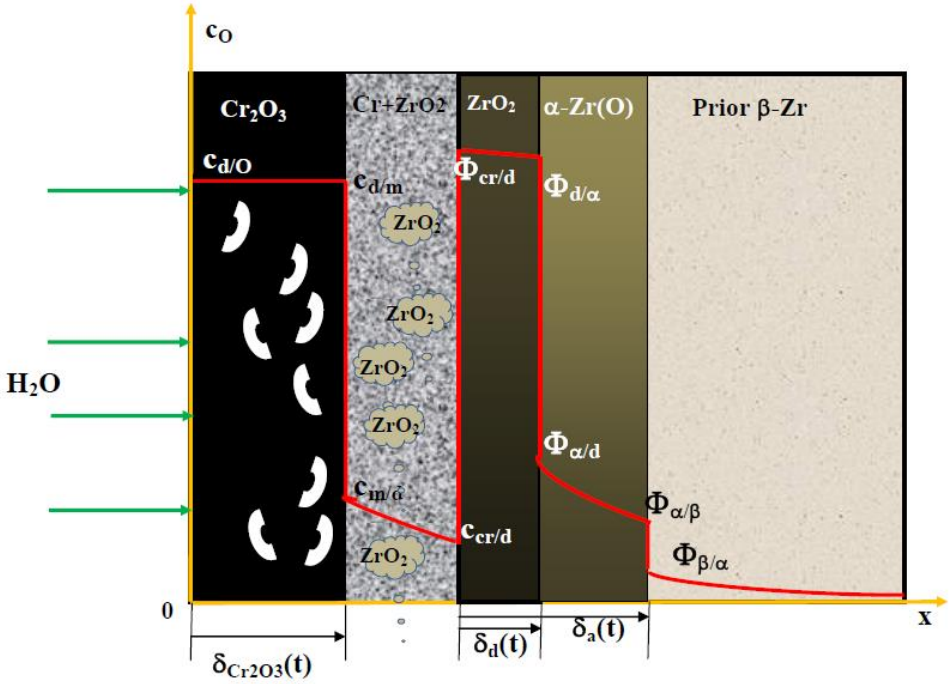

Figure 4: The profile of oxygen concentration in the course of phase III. The oxide layer Cr_2O_3 and the metallic Cr layer have already lost their protective as it was discussed in previous section. The three-layer system of layers in Zr substrate is supposed

The solution for ZrO_2/α-*Zr*(*O*) and α-*Zr*(*O*)/β-*Zr* interface coordinates (Fig. 4) are represented as following [10]:

$$\delta_d = K_d\sqrt{t}\ ,\ \delta_a = K_a\sqrt{t}\ , \tag{7}$$

$$\frac{K_a}{\sqrt{4D_a}} \cong 1$$

$$\frac{K_d}{\sqrt{4D_d}} \cong \frac{-\left(\Phi_{\frac{\alpha}{d}} - \Phi_{\frac{\alpha}{\beta}} r_{Zr}\right)\sqrt{\frac{D_a}{D_d}} + \sqrt{\left(\Phi_{\frac{\alpha}{d}} - \Phi_{\frac{\alpha}{\beta}}\right)^2 \frac{D_a}{D_d} + 8A^2\left(\Phi_{\frac{d}{\alpha}} - \Phi_{\frac{\alpha}{d}} r_{Zr}\right)\left(\Phi_{\frac{cr}{d}} - \Phi_{\frac{d}{\alpha}}\right)}}{4A\left(\Phi_{\frac{d}{\alpha}} - \Phi_{\frac{\alpha}{d}} r_{Zr}\right)}, \tag{8}$$

$$A = \int_0^{\frac{K_a}{\sqrt{4D_a}}} e^{-y^2} dy.$$

Here the Bedworth-Pilling ratio for zirconium is $r_{Zr} = \left(\rho_{ZrO_2}/\rho_{Zr}\right)\cdot\left(2\mu_{Zr}/\mu_{ZrO_2}\right)$, Φ - the corresponding interface oxygen densities [kg/m^3], D_d and D_a – the oxygen diffusion coefficients in oxide and metal α-phase respectively.

3 MODELLING OF FECRAL OXIDATION AT HIGH TEMPERATURES

For modelling of high-temperature oxidation of a cladding made of *FeCrAl* alloy we can use the parabolic model. The parabolic oxidation constant for weight gain of *FeCrAl* sample is approximated as [14]

$$K = 28.3 \cdot e^{-\frac{16150}{T}}\ \text{kg/(m}^2\text{s}^{0.5}\text{)} \tag{9}$$

We can also use in this case the Eqs. (1,2) with corresponding effective oxygen diffusion coefficients and interface concentrations.

For the consideration of enhanced oxidation rate near the melting point of *FeO* we can introduce the oxygen diffusion enhancement factor K_{diff} that is $D_{eff,ox} = K_{diff}.D_{standard,ox}$. So, the parabolic rate for weight gain in the vicinity of melting point will be estimated approximately as $K_{eff} \approx K \cdot \sqrt{K_{diff}}$.

The application of this methodology to the modelling of integral experiment QUENCH-19 [8] will be presented below in the Section 5.

4 DEVELOPMENT OF NUMERICAL CODE AND RESULTS OF MODELLING

The numerical code SFPSA was developed to calculate the diffusion equations for oxygen in multilayer structures, Figs 2-4.

We are looking for a solution of following diffusion equations in each layer:

$$\frac{\partial \Phi}{\partial t} = \frac{\partial}{\partial x}\left(D_i \frac{\partial \Phi}{\partial x}\right), \qquad \delta_{il}(t) < x < \delta_{ir}(t)\ , \tag{10}$$

where $\Phi=c_O$, kg/m^3, is the oxygen concentration; the diffusion coefficient D_i, m^2/s, is a function of layer name (Cr_2O_3, *Cr*, ZrO_2, α-*Zr*(O), β-*Zr*) and the temperature *T*, K; δ_{il} and δ_{ir} are the left and right coordinates of given layer *i*, respectively. Corresponding initial and boundary conditions should be added to Eq. (10) for completeness.

Due to discontinuity of the concentration and its derivative on coordinate x it is very convenient to use a special function.

Let us introduce a new function $\Re(\Phi)$ (the Kirchhoff transformation on oxygen concentration Φ):

$$\Re(\Phi) = \int_{\Phi_0}^{\Phi} d\Phi' \frac{D(\Phi)}{D(\Phi_0)} . \quad (11)$$

This new function also satisfies to diffusion Eqs (10) but is continuous at the boundaries between different layers. The first derivative of this function on coordinate is continuous, too. After numerical solution of diffusion equations for Kirchhoff transformation with corresponding interface boundary conditions we will get the function $\Re$ in all one-dimensional space. After that it will be very easy to transform $\Re$ it back to oxygen concentrations Φ.

For calculation of second derivative on length coordinate the following operator is used:

$$\Lambda(\Re) = \frac{1}{h}[D_{i+1}\cdot(\Re_{i+1} - \Re_i)/h - D_i\cdot(\Re_i - \Re_{i-1})/h] , \quad (12)$$

where *h* is the space length step, *i* is a spatial index along the *x*-coordinate.

So, we will get a solution at a new time step using approximation

$$(\Re_i^{n+1} - \Re_i^n)/\tau = \Lambda[\sigma\cdot\Re_i^{n+1} + (1-\sigma)\cdot\Re_i^n)] \quad (13)$$

where *n* is the current time index and *n*+1 is the next time index; σ is the semi-implicitness parameter. The numerical solution for function $\Re$ is very easy due to its continuity.

The model can also be applied for oxidation of *FeCrAl* claddings. To do this we should add the corresponding input parameters for *FeCrAl* into the code.

5 RESULTS OF MODELLING

Some results of numerical modelling and the comparison with the experimental data are presented below, see Fig. 5. The isothermal experiment [9] with Cr-coated *Zry*-4 cladding oxidation conducted recently at KIT, Karlsruhe, Germany, is chosen for modelling. The experimental data clearly show the initial growth of Cr_2O_3 layer (Phase I, t=0÷2000 s). Then, the thinning of protective Cr_2O_3 layer is observed (Phase II, t=2000÷7200 s).

We see that the new code developed and presented in this paper predicts the experimental behaviour pretty well. The second term in right hand of Eq. (5) ensures the initial parabolic growth of chromium oxide layer. Then, the third term in right hand of Eq. (5) begins to prevail and we observe the thinning of the chromium oxide layer. Correspondingly, the oxygen flux to the sample increases leading to transition from parabolic to linear oxidation kinetics (Phases II and III). The ZrO_2 layer begins to form (observed in this experiment) which means the loss of protective properties of chromium-coated *Zry*-4 cladding.

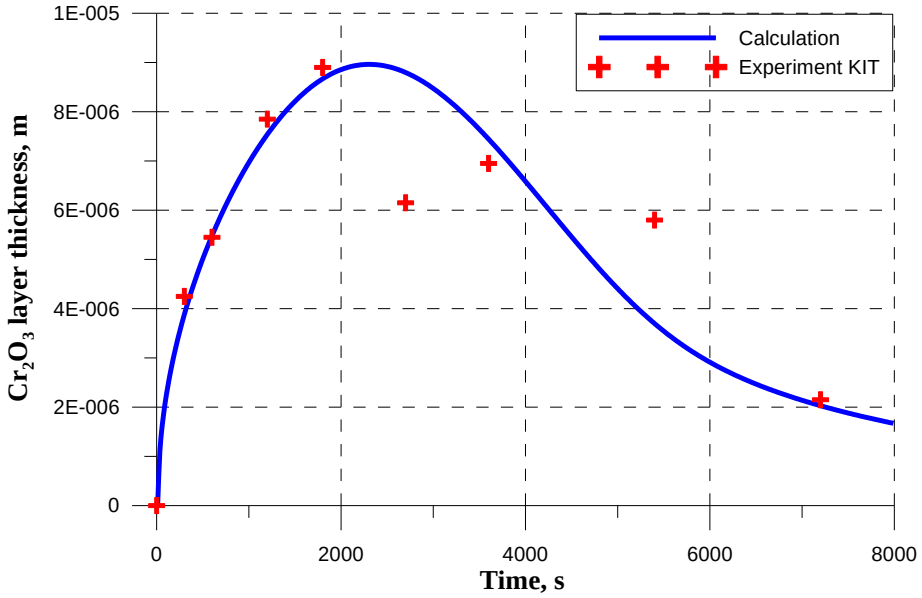

Figure 5: Chromium oxide thickness: the results of numerical calculation (blue line) compared to experimental dynamics (KIT, Karlsruhe) reproduced from the paper [9]. *Cr*-coated *Zry*-4 sample at *T*=1200°C

Now consider the modelling of the integral experiment QUENCH-19 conducted at KIT, Karlsruhe, Germany [8]. We use a special fast running code SFPSA developed for modelling of severe accident conditions and solving the diffusion equations considered in Section 4. The results of modelling with the standard correlation (Eq. 9) and the effective enhanced oxygen diffusion coefficient in oxide layer $D_{eff,ox} = K_{diff} \cdot D_{standard,ox}$ are shown in the Fig. 6.

One can see that the application of standard parabolic constant (standard value of oxygen diffusion coefficient $D_{standard,ox}$ in the oxide layer) results in large underestimation of integral hydrogen generation in the test.

The use in the code of enhanced diffusion coefficient leads to adequate modelling of H_2 production in the QUENCH-19 test. It was supposed that the parameter K_{diff} was linearly enhanced in time from $K_{diff} = 1$ to $K_{diff} = 6$, beginning from the time moment when the temperature at elevation 950 mm (the maximum temperature in the bundle) reached *T*=1250°C. This period continued till the reflood initiation. The duration of this period was about 100 s.

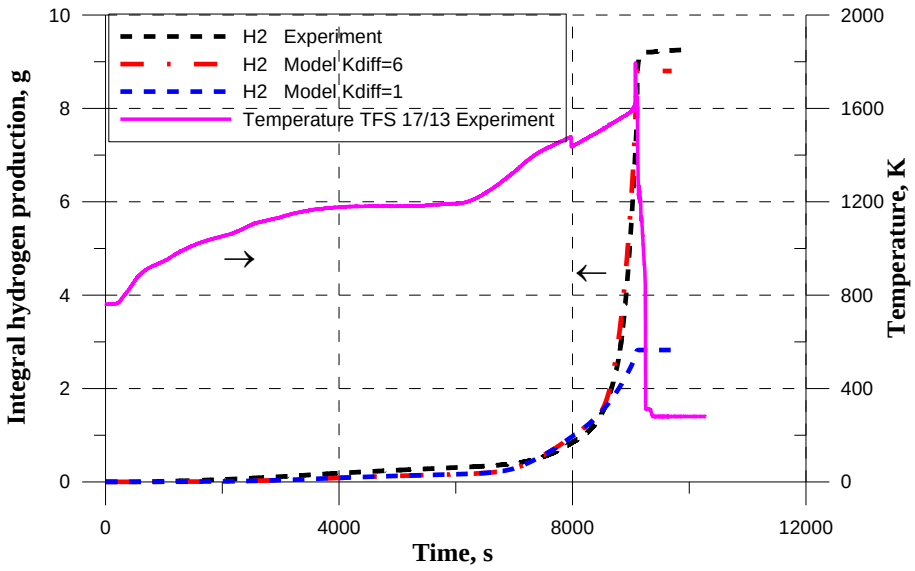

Figure 6: Integral H_2 generation in the experiment QUENCH-19 with *FeCrAl* claddings: the calculation and experimental data

6 CONCLUSIONS

In this paper, the new advanced analytical models of high-temperature oxidation of perspective ATF-claddings on the basis of *FeCrAl* alloy and zirconium-based alloy claddings with chromium coating are described. For consideration of Zr/Cr cladding, the model is based on the solution of oxygen and zirconium diffusion equations in a system of layers formed in the course of oxidation. The model takes into account a number of important processes influencing the oxidation behavior in a system *Zr*/*Cr*. The model developed is implemented to numerical computer-running code. In the case of *FeCrAl* the diffusion model is proposed taking into account dramatic enhancement of oxygen diffusion coefficient at high temperatures approaching the melting point of FeO.

The comparison of calculated results for *Zr/Cr* cladding high temperature oxidation with experimental data is presented. The recent experimental data from the QUENCH-19 experiment with *FeCrAl* claddings and from the *Cr*-coated *Zry*-4 oxidation test at the temperature T=1200°C obtained in KIT, Karlsruhe, Germany, are chosen for validation of the model developed. Despite the exclusive complexity of phenomena involved, the reasonable agreement between calculated and experimental data is observed. It demonstrates the predictive ability of the model developed.

It seems that the subject of special attention is the approaching to the temperatures about T=1250°C in the case of *FeCrAl* cladding and about T=1200°C in the case of *Zr/Cr* cladding when the protective properties of oxide layers are dramatically weakened.

The upper temperature limit of design-basis-accident is T=1200°C, and at this temperature we observe the worsening of protective properties of oxides formed on claddings. On the whole, it seems that the application of ATF *FeCrAl* and zirconium-based cladding with chromium coating for commercial NPPs looks reasonable because of saving time and the principal possibility of exclusion of nuclear reactor accident escalation from design-basis-accident to beyond-design-basis-accident.

Currently, the search for ATF-cladding materials with good corrosion and oxidation resistance characteristics is underway in the important temperature range $T \geq 1200$°C.

ACKNOWLEDGMENTS

The author would like to acknowledge Prof. L.Matveev from IBRAE, Moscow, for the fruitful discussions.

REFERENCES

[1] K.Terrani, “Accident tolerant fuel cladding development: promise, status, and challenges”, J. of Nuclear Materials, 501, 2018, pp. 13-30.

[2] J.-Ch. Brachet, E. Rouesne, J. Ribis, T. Guilbert, S. Urvoy, G. Nony, C. Toffolon-Masclet, M. Le Saux, N. Chaabane, H. Palancher, A. David, J. Bischoff, J. Augereau, E. Pouillier, “High temperature steam oxidation of chromium-coated zirconium-based alloys: kinetics and process”, Corrosion Science, 167, 2020, 108537, 15 pp. Online version: https://doi.org/10.1016/j.corsci.2020.108537.

[3] P. Vrbka, J. Krejci, J. Kabatova et al., “Air oxidation of sponge based E110 cladding alloy at high temperatures”, Proc. 23th International QUENCH Workshop (QUENCH-23), Karlsruhe, Germany, October 17-19, 2017.

[4] V. Avincola, “Oxidation and quench of silicon carbide composites in high temperature corrosive environments”, Proc. 20th International QUENCH Workshop (QUENCH-20), Karlsruhe, Germany, November 11-13, 2014.

[5] M. Steinbrueck, “High-temperature oxidation of SiC-Ta-SiC sandwich cladding tubes in GFR atmosphere”, Proc. 22nd International QUENCH Workshop (QUENCH-22), Karlsruhe, Germany, October 18-20, 2016.

[6] K.G. Field, M.A. Snead, Y. Yamamoto, K.A. Terrani, “Handbook on the material properties of FeCrAl alloys for nuclear power production applications”, August 2018, ORNL/SPR-2018/905, US.

[7] J.-H. Park, H.-G. Kim, J.-Y. Park, Y.-I. Jung, D.-J. Park, Y.-H. Koo, “High temperature steam-oxidation behavior of arc ion plated Cr coatings for accident tolerant fuel claddings”, Surface & Coatings Technology, 280, 2015, pp. 256-259.

[8] P. Doyle, Ju. Stuckert, M. Grosse, V, Steinbrueck, A. Nelson, J. Harp, K. Terrani, “Analysis of iron-chromium-aluminum samples exposed to accident conditions followed by quench in the QUENCH-19 experiment”, J. of Nuclear Materials, 580, 2023, 154433, 15 pp.

[9] Saber D., I.S. Emam, R. Abdel-Karim, “High Temperature Cyclic Oxidation of Ni Based Superalloys at Different Temperatures in Air”, J. of Alloys and Compounds, 719, 2017, pp. 133-141.

[10] A. Vasiliev, “High-temperature oxidation modeling of new perspective accident tolerant fuel claddings”, Proc. 2019 ASME International Mechanical Engineering Congress and Exposition (IMECE2019), Salt Lake City, Utah, US, November 11-14, 2019, IMECE2019-10513.

[11] A.D. Vasiliev, "Analytical Modelling of ATF Chromium-Coated Zr-Based Cladding High Temperature Oxidation in Steam and Steam-Air Atmosphere", Proc. Int. Conf. “Nuclear Energy for New Europe 2021”, Portorož, Slovenia, September 6-9, Nuclear Society of Slovenia, 2021, NENE-2021-416.

[12] J. Liu, U. Stegmaier, C. Tang, M. Steinbrueck, M. Grosse, “The coating degradation mechanism during the isothermal steam oxidation of Cr-coated Zry-4 at 1200°C”, Proc. 26th International QUENCH Workshop (QUENCH-26), Karlsruhe, Germany, December 6-10, 2021.

[13] A. D. Vasiliev, “Advanced model of Zr-based claddings oxidation in steam-oxygen-nitrogen gas mixtures embracing all range from low to high temperatures”, Proc. SAFEST Air Oxidation Meeting “Cladding Oxidation by Air under Severe Accident Conditions in a Nuclear Reactor and a Spent Fuel Pool”, Budapest, Hungary, June 14-15, 2016.

[14] Zhong W., Mouche P.A., Han X. et al. Performance of Iron-Chromium-Aluminium Alloy Surface Coatings on Zircaloy 2 under High-Temperature Steam and Normal BWR Operationg Conditions. J. of Nuclear Materials, 2016, V. 470, pp. 327-338.

[15] A. Vasiliev, “Post-Test Modelling of the Experiment QUENCH-19 with FeCrAl Cladding Material Using SOCRAT Code”, Proc. 25th International QUENCH Workshop (QUENCH-25), Karlsruhe, Germany, October 22-24, 2019.